Available online at www.sciencedirect.com
ScienceDirect
Tectonophysics 431 (2007) 97–111
TECTONOPHYSICS
www.elsevier.com/locate/tecto

Indicators of critical point behavior prior to rock failure inferred from pre-failure damage

Xinglin Lei *, Takashi Satoh

Institute of Geology and Geoinformation/GSJ, National Institute of Advanced Industrial Science and Technology, AIST Central #7, Higashi 1-1-1, Tsukuba, Ibaraki, 305-8567 Japan

Received 16 January 2006; received in revised form 18 April 2006; accepted 28 April 2006
Available online 7 November 2006

Abstract

To investigate possible indicators of critical point behavior prior to rock failure, the statistical properties of pre-failure damage were analyzed based on acoustic emission events (AE) recorded during the catastrophic fracture of typical rock samples under differential compression. AEs were monitored using a high-speed 32-channel waveform recording system. Time-dependent statistics, including the energy release rate, *b*-value of the magnitude–frequency distribution, fractal dimension and spatial correlation length (SCL) of the AE hypocenters were calculated for each data set. Each parameter is a function of the time-to-failure and thus can be treated as an indicator of the critical point. It is clear that the pre-failure damage evolution prior to catastrophic failures in several common rock-types is generally characterized by: 1) accelerated energy release, 2) a decrease in fractal dimension and SCL with a subsequent precursory increase, and 3) a decrease in *b*-value from ~1.5 to ~0.5 for hard rocks, and from ~1.1 to ~0.8 for soft rocks such S–C cataclasite. However, each parameter also reveals more complicated temporal evolution due to either the heterogeneity of the rock mass or the micro-mechanics of shear fracturing. This confirms the potential importance of integrated analysis of two or more parameters for successfully predicting the critical point. The decreasing *b*-value and increasing energy release may prove meaningful for intermediate-term prediction, while the precursory increase in fractal dimension and SCL may facilitate short-term prediction.

Keywords: Acoustic emission; Microfracturing; Fractals; *b*-value; Critical phenomena

1. Introduction

It is well known that before and after relatively large earthquakes, seismic activity surrounding the source area exhibits generally higher activity than the long-term background. Seismologists have therefore tried to predict large events by quantitative analysis of such increases in seismic activity. Most earthquakes occur on pre-existing faults, which generally comprise cracks at many different scales. In addition, the crust as a whole shows heterogeneities at many scales. As a result, earthquakes do not represent pure stick–slip failures on the fault surface but also involve some form of rock fracture. This means that the fracturing process must be investigated at all scales in order to fully understand seismic source mechanics (Kagan and Jackson, 1991). Current earthquake prediction methodologies can be classified into two groups based on their treatment of either the frictional behavior of individual faults or rock fracture within the fault zone and surrounding region. The former addresses pre-slip

* Corresponding author. Institute of Geology & Sate Key Laboratory of Earthquake Dynamics, China Seismological Administration, Beijing, China.
E-mail addresses: xinglin-lei@aist.go.jp (X. Lei), t.satoh@aist.go.jp (T. Satoh).
URL: http://staff.aist.go.jp/xinglin-lei/ (X. Lei).

0040-1951/$ - see front matter © 2006 Elsevier B.V. All rights reserved.
doi:10.1016/j.tecto.2006.04.023

behavior by means of numerical simulation incorporating laboratory-derived friction laws, whereas the latter considers the statistical properties of micro-earthquakes in the crust or the pre-failure damage caused by microcracks at laboratory scales.

Abundant experiment evidence reveals that macroscopic shear failure in rocks and other brittle materials does not take place by the growth of a single shear crack in its own plane, but is in fact preceded by a very complex and pervasive evolution of pre-failure damage in the rock (e.g. Lei et al., 2000b). Progress towards modeling both the damage evolution and subsequent fracturing dynamics has been made using a combination of experimental and theoretical approaches. The concept of critical point behavior has been applied to earthquakes, rockbursts (e.g. Ouillon and Sornette, 2000), and acoustic emissions (e.g. Andrë et al., 2005) using time-to-failure analysis. Here, the catastrophic event is considered to be a critical phenomenon occurring at a second-order phase transition in analogy to percolation phenomena (Yamashita and Knopoff, 1989; Sornette and Sornette, 1990).

If a system approaches a critical point, the spatial correlation length (hereafter abbreviated as SCL) is expected to grow according to a power law (Bruce and Wallace, 1989):

$$\xi(t) \propto (t_f - t)^{-k} \quad (1)$$

where k is positive. Using single-link cluster analysis (Frohlich and Davis, 1990), Zöller et al. (2001) conducted a systematic analysis of all earthquakes with $M \geq 6.5$ in California since 1952 and found that k has a value of 0.24–0.57. Tyupkin and Giovambattista (2005) performed correlation length analysis of acoustic emission events recorded in laboratory rock deformation experiments and SCL analysis of intermediate magnitude earthquakes in the areas surrounding subsequent large earthquakes in Kamchatka and Italy. That study's results revealed a decrease in SCL preceding precursory growth before large events.

Assuming a scaling relation between moment release E and SCL, growing SCLs (GSCLs) imply the following accelerated moment release (AMR) model:

$$\Sigma \sqrt{E(t)} = A + B(t_f - t)^m \quad (2)$$

Here the sum represents the cumulative Benioff strain, and t_f is the failure time of the large event (see review by Jaume and Sykes, 1999). Bufe and Varnes (1993) and Bufe et al. (1994) found that the clustering of intermediate events before a large earthquake produces a regional increase of moment release, as predicted by the AMR model for $m \sim 0.3$. In the New Madrid seismic zone, the value $m = 0.13$–0.47 was proposed by Brehm and Braile (1998, 1999). Subsequent work has suggested an empirical relation between the logarithm of the critical region radius (R) and the magnitude of the final event (M), $\log R \propto dM$, where d is a scalar variably suggested to be 0.44 by Bowman et al. (1998), 0.75 by Brehm and Braile (1998), 0.36 by Jaume and Sykes (1999), and 0.5 by Zöller et al. (2001). More recently, AMR has been linked with Coulomb stress interactions (Bowman and King, 2001).

On the other hand, when the catastrophic event is treated as a critical point, the fracturing process can be

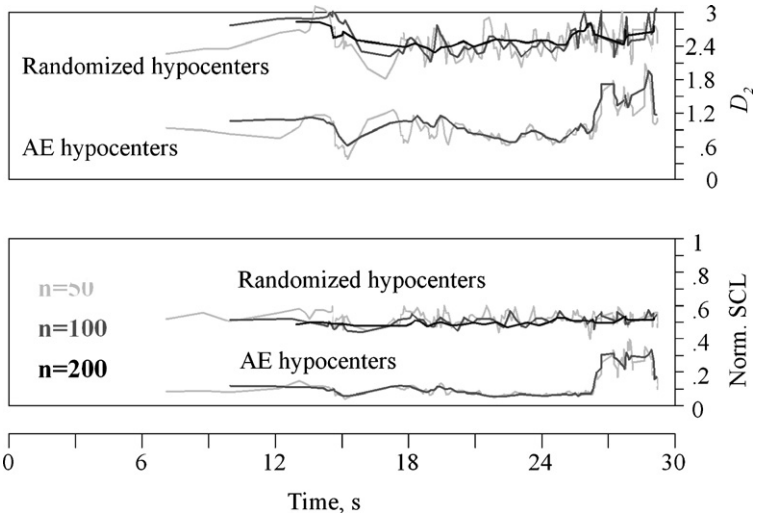

Fig. 1. Fractal dimension and SCL of the AE hypocenters and random data, illustrating the method of checking the results' dependence on the number of events analyzed.

described using a renormalization-group scheme (Anifrani et al., 1995). In the vicinity of the critical point, there exists a critical region in which variations of the energy release can be characterized by a power-law time-to-failure relationship (similar to AMR) characterized by log-periodic oscillations (Sornette, 1998). Mathematically, such oscillations correspond to adding an imaginary part to the exponent of the AMR model.

$$\Sigma\sqrt{E(t)} = A + B(t_c - t)^{\alpha+i\omega} \tag{3}$$

Here A, B, α, and ω are constant, t_c represents the critical point, in other word, the global failure time. The log-periodic oscillations result from heterogeneities in the system and are a measure of interaction (Andrë et al., 2005). They correspond to an accelerating frequency modulation as the critical time is approached, and thus are useful for prediction purposes. It should be noted that Eq. (3) is valid only at the critical region, i.e. $t \to t_c$. By employing self-similar approximation theory, the general law of energy release that is also valid outside the critical region can be derived (Yukalov et al., 2004). The dimensionless form is given by:

$$\frac{E(x=(t_c-t)/t_c)}{E(x=0)} \approx f^*(x), \qquad x\epsilon[0,1]$$
$$f^*(x) = \cos(cx^\alpha \sin g(x)\exp h(x)) \times \exp(cx^\alpha \cos g(x)\exp h(x)) \tag{4}$$

where

$$g(x) = a\sin(\omega \ln x) + b\cos(\omega \ln x)$$
$$h(x) = a\cos(\omega \ln x) - b\sin(\omega \ln x) \tag{5}$$

and a,b,c are unknown parameters.

Power-law energy release has been linked with growth of the mean crack length based on stress corrosion constitute laws (e.g. Main et al., 1993; Lei,

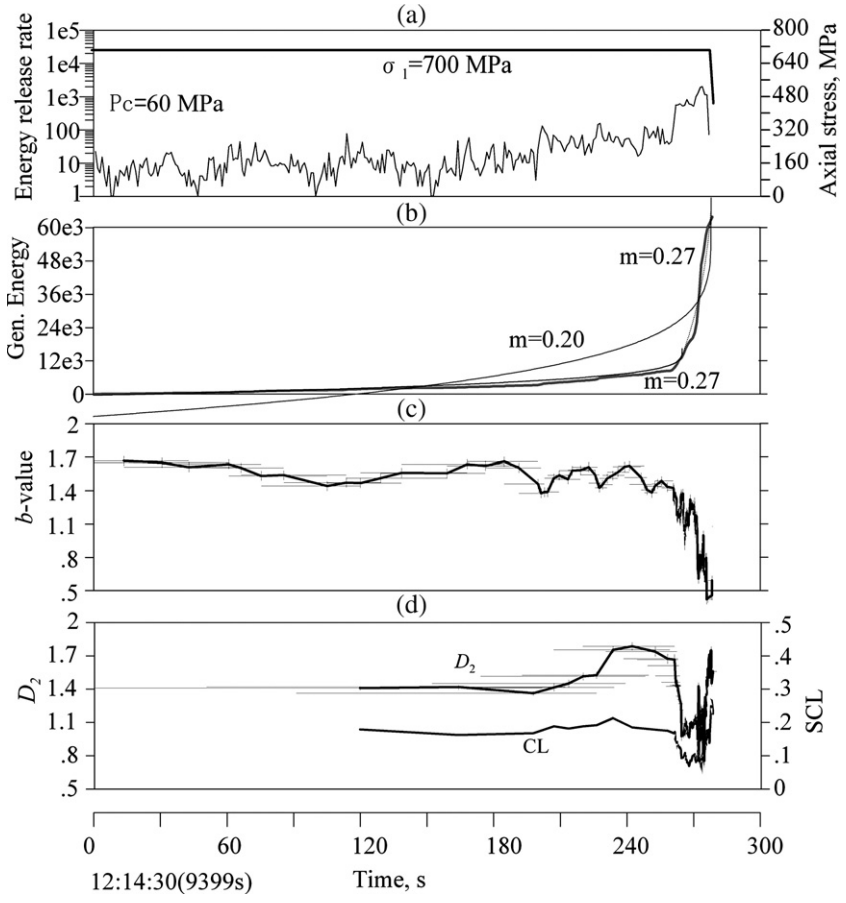

Fig. 2. Results for a fine-grained hornblende schist sample. a) Axial stress and generalized energy release rate. b) Generalized cumulative energy and the theoretical estimation using multi-domain power-law fits. c) b-values calculated sequentially for consecutive groups of 500 events with an increment of 125 events. The vertical and horizontal bars indicate the standard error and time window, respectively. d) Fractal dimension D_2 and SCL of the AE hypocenters calculated sequentially for consecutive groups of 100 hypocenters with an increment of 25 hypocenters.

2006). Such models can explain both the increasing energy release and the decreasing *b*-values in the magnitude–frequency relation (Lei, 2006). Plausible physical mechanics have also been proposed for some precursory anomalies such as quiescence (Main and Meredith, 1991) and *b*-value anomalies associated with large earthquakes (Main et al., 1989).

Experimental results obtained by Andrë et al. (2005) showed for the first time that the imaginary part of the complex critical exponent ω is correlated with loading rate and heterogeneity due to grain size distribution. This confirms that the larger the dominant grain size or the faster the loading rate, the longer the interaction, and the higher the exponent ω. Therefore, laboratory studies are helpful for understanding the physical mechanisms behind the statistical models and thereby improving their predictability.

In this paper, we report on new tests performed on AE catalogs obtained in laboratory experiments of fracture of several rocks. We focus on the simultaneous analysis of energy release, volumetric strain, seismic *b*-value, fractal dimension and spatial correlation length. These parameters are useful for connecting experimental studies at laboratory scale and geophysical studies at large scale.

2. Experiments and data processing procedures

Detailed descriptions of the experimental setup can be found in our previous papers (e.g. Lei et al., 2000a; Lei, 2006) but it may be helpful to briefly summarize some important points here. Cylindrical rock samples, 50 mm in diameter and 125 mm in length, are placed in a pressure vessel, which is then inserted in a loading frame. Hydraulic oil is used as the confining pressure medium. AE waveforms are recorded with 32 compressional-mode piezoelectric transducers (PZTs; 1 MHz resonant frequency, 5 mm in diameter) mounted on the surface of the test sample, using a high-speed recording system. In addition to the waveforms, the maximum amplitudes at two artificially selected sensors are recorded separately and used to calculate the magnitude and energy of AE events. AE hypocenters are determined from the first P-arrival times.

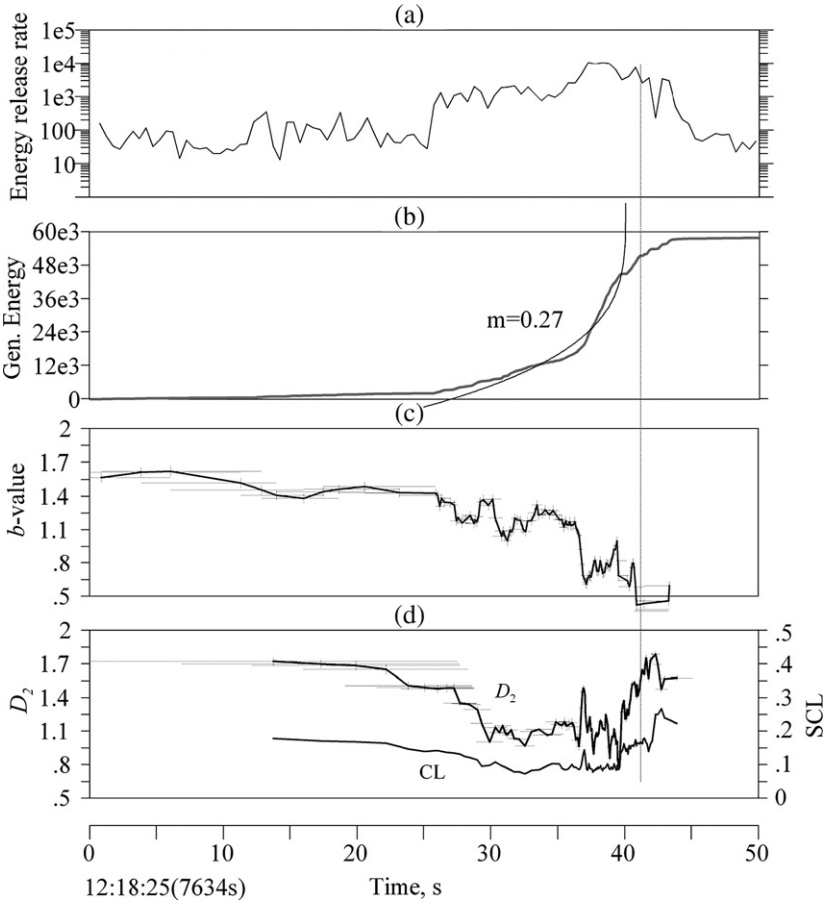

Fig. 3. Close up view of the final 50 s of the experiment illustrated in Fig. 2.

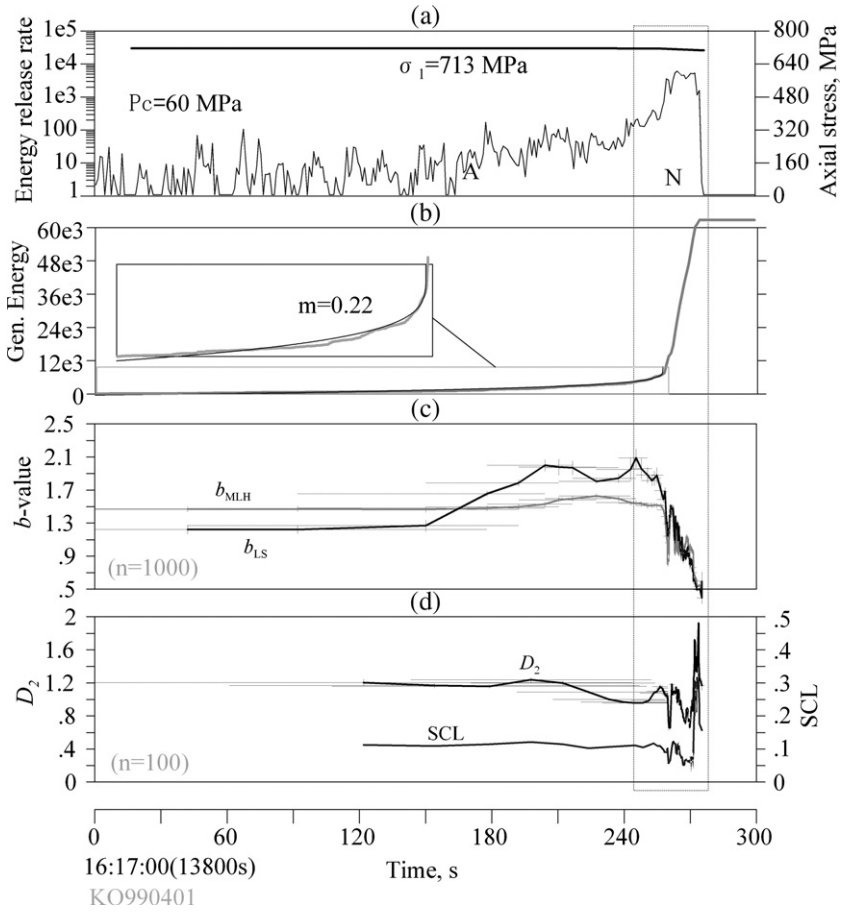

Fig. 4. Results for another fine-grained hornblende schist sample. a) Axial stress and generalized energy release rate. b) Generalized cumulative energy and the theoretical estimation of multi-domain power-law fits. c) *b*-values calculated sequentially for consecutive groups of 500 events with an increment of 125 events. The vertical and horizontal bars indicate the standard error and time window, respectively. d) Fractal dimension D_2 and SCL of the AE hypocenters calculated sequentially for consecutive groups of 100 hypocenters with an increment of 25 hypocenters.

Hypocentral errors are estimated to be generally less than 1–2 mm for fine-grained rocks and slightly greater for coarse-grained rocks (Lei et al., 2000b, 2004). It is important to emphasize that during each test, the trigger threshold for waveform recording is about 10 times larger than the threshold for the detection of the maximum amplitude. As a result, the hypocenter data constitute a subset of the magnitude data. Eight cross-type strain gauges are mounted on the surface of the test samples: these are used to measure the local strains along the axial and circumferential directions. The mean strains of the test samples are estimated by averaging these local measurements.

In this paper, the fundamental data are AE magnitude, AE hypocenter, and volumetric strain. The statistical parameters computed from these observations are 1) the energy release rate and cumulative energy release, 2) the *b*-value of the frequency–magnitude distribution, and 3) the fractal dimension and SCL of the AE hypocenters.

According to Lei et al. (2003), the recorded AE signal is roughly proportional to the vibration velocity of the elastic wave. Following the definition of the body-wave earthquake magnitude, the magnitude (M) of each AE event can be determined in a relative sense using the logarithm of the AE signal's maximum amplitude ($V_{\max}$):$M \propto \log V_{\max} = A_{db}20$, where A_{dB} is the maximum amplitude in dB. As a result of the unknown calibration parameter, the non-flat response, and distance-dependent attenuation, the magnitudes that are obtained in this way ought to be considered only as first-order approximations of the relative values. As with earthquakes, the energy of each AE event can be defined by

$$E_i \propto 10^{CM_i} \tag{6}$$

where C is a constant. The most important cases are $C=0.75$ and 1.5, which correspond to the Benioff strain and the classic energy release, respectively.

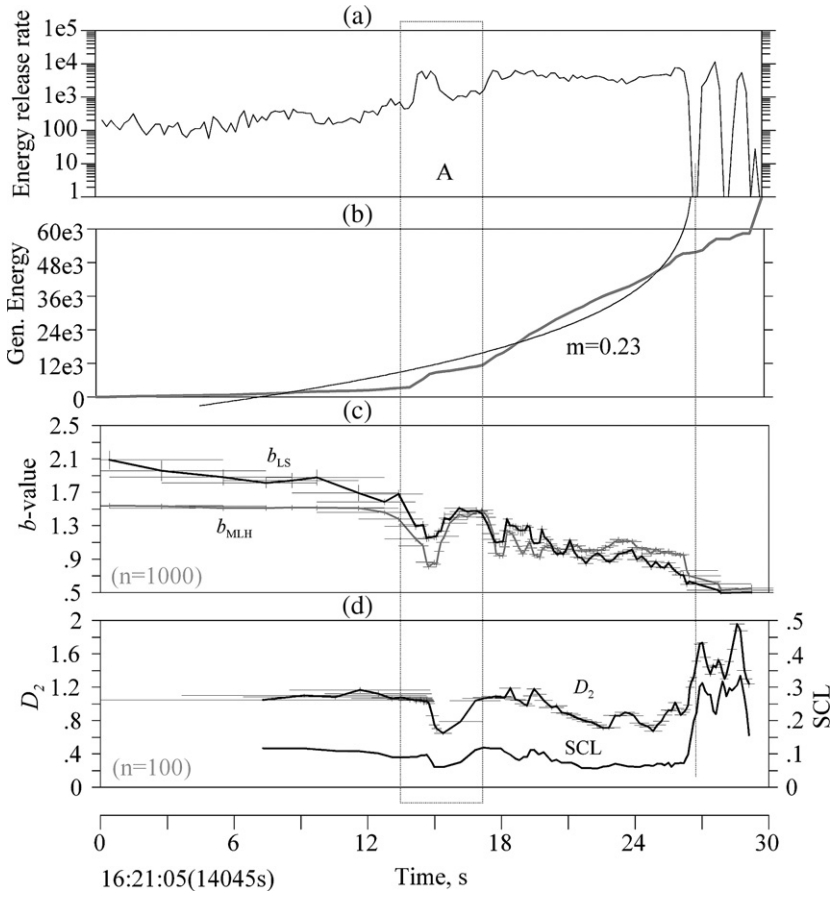

Fig. 5. Close up view of the final 30 s of the experimental run illustrated in Fig. 4.

2.1. Energy release and b value

The energy release rate can be estimated by summing Eq. (6) within a given unit time interval (Δt):

$$\dot{E}(t) = \Sigma E_i/\Delta t \tag{7}$$

The cumulative energy release can be simply defined by:

$$\Sigma E = \int \dot{E} dt \tag{8}$$

In this paper, C=0.75 (which yields the Benioff strain) was used in the calculation of energy release rate and cumulative energy release.

The archetypal power-law found in earthquake catalogs is the Gutenberg-Richter magnitude–frequency relationship. It also holds for AE events in rock samples (e.g., Scholz, 1968; Liakopoulou-Morris et al., 1994). The cumulative event number (n) of magnitude M or greater is a function of magnitude given by

$$\log_{10} n = a - bM \tag{9}$$

(Gutenberg and Richter, 1954). In Eq. (9), a and b are constant, and b is referred to as the b-value. For the experimental results presented here, the b value was sequentially calculated for consecutive groups of 500 or 1000 events with an increment of 125 or 250 events.

2.2. Fractal dimension and SCL of AE hypocenters

In a similar manner to earthquakes, AE hypocenters are generally distributed throughout rock samples as clusters and can be quantified using a fractal dimension. Here, the correlation integral was used (Hirata, 1987):

$$C(r) = \frac{2N_r(R<r)}{N(N-1)} \tag{10}$$

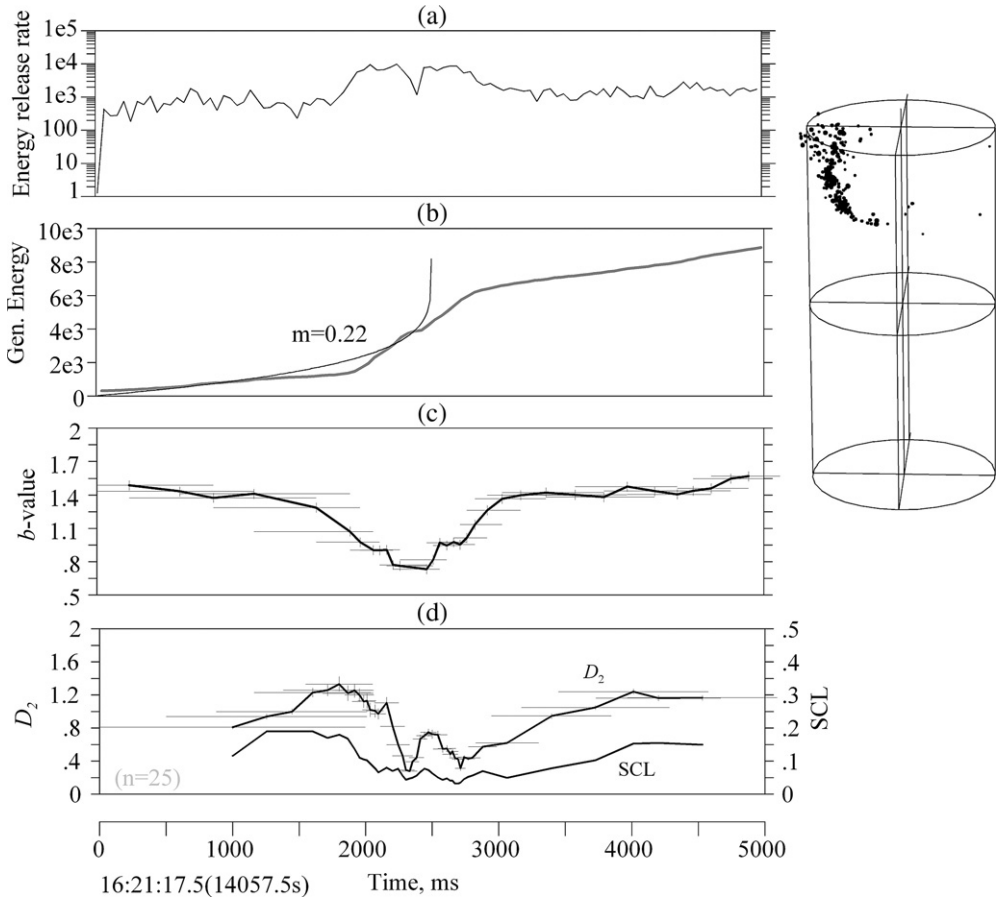

Fig. 6. Close-up views of the period marked 'A' in Fig. 5, corresponding to a dense AE cluster. A simple power-law fit has been performed on the cumulative energy release data associated with a few large events occurring near the peak of the energy release curve. The spatial distribution of AE hypocenters is plotted on the right-hand side.

$Nr(R<r)$ is the number of AE hypocenter pairs separated by a distance smaller than r, and N is the total number of AE events analyzed. If the hypocenter distribution exhibits fractal characteristics, then $C_q(r)$ is a power-law function of r, namely $C_q(r) \propto r^{D2}$. Here, D_2 defines the correlation dimension.

In addition to the fractal dimension, the SCL can also be used to characterize the spatial distribution of AE hypocenters. The SCL of a set of N consecutive events is estimated using single-link cluster analysis (Frohlich and Davis, 1990). Initially, each individual hypocenter is linked with its nearest neighbor hypocenter to form a set of clusters. Then, every cluster is linked with its nearest cluster. This process is repeated until N events are connected with $N-1$ links. Throughout the process, the distance between any two clusters is calculated based on their geometric centers. Following previous work (Zöller et al., 2001; Tyupkin and Giovambattista, 2005), the SCL is here defined as the median of the length distribution of the $N-1$ links. In order to reduce the dependence of SCL on event number and sample dimension, we use the dimensionless value given by

$$\xi_R(t) = \xi(t)/l_R \qquad l_R = l_\Omega/n^{1/3} \tag{11}$$

where l_Ω is the characteristic linear dimension of the rock sample, or 50 mm in our case.

In order to examine the dependence of the fractal dimension and SCL on the number of events, and thus the measurements' significance, clustered AE hypocenters and artificially created random data were tested in tandem. The random data was created from the AE data by replacing the coordinates of each hypocenter with computer-generated random values. For both data sets, the fractal dimension D_2 and SCL were sequentially calculated for consecutive groups of N events (N=25, 50, 100, 200) with an increment of $N/4$ events. Fig. 1 confirms that $N \geq 25$ results in good estimations of both D_2 and SCL

for the clustered AE hypocenters. However, for the randomized data, results for $N \leq 50$ are noisy, especially for D_2. In the present paper, $N \geq 100$ is generally used. $N=25$ or 50 is also used to illustrate the detailed temporal evolution of densely clustered AE events.

3. Rock samples

We performed new tests on the AE catalogs obtained during rock fracture tests performed on the following common lithologies:

1) Fine-grained hornblende schist collected from the Kolar Gold Mine, which has been examined systematically by Lei et al. (2000a). The hornblende schist has very fine grain size (0.2–0.7 mm) and a very high strength of >700 MPa at confining pressures of 60 MPa. It also exhibits very brittle behaviors without notable strain softening.
2) Coarse-grained Tsukuba granite, collected from drill cores in the Tsukuba Mountain, Kanto, Japan. The predominant grain size exceeds 10 mm. Tsukuba granite has a strength of approximately 550 MPa under confining pressures of 60 MPa and behaves brittlely with minor strain softening.
3) Coarse-grained S–C cataclasite, collected from drill cores in the Nojima fault zone at depths of 195–216 m, near where the 1995 M7.2 Kobe earthquake occurred. The predominant grain size ranges from 3 to 5 mm. The S–C cataclasite has very low strength of <200 MPa at confining pressures of 40 MPa and shows significant strain softening.
4) Mudstone samples, collected from drill cores retrieved from depths of about 980 m in central Japan and containing sporadic 1–3 mm-thick quartz veins. The general fracture behavior of similar lithologies was investigated by Lei et al. (2000c), who found that the quartz veins play a role in controlling the

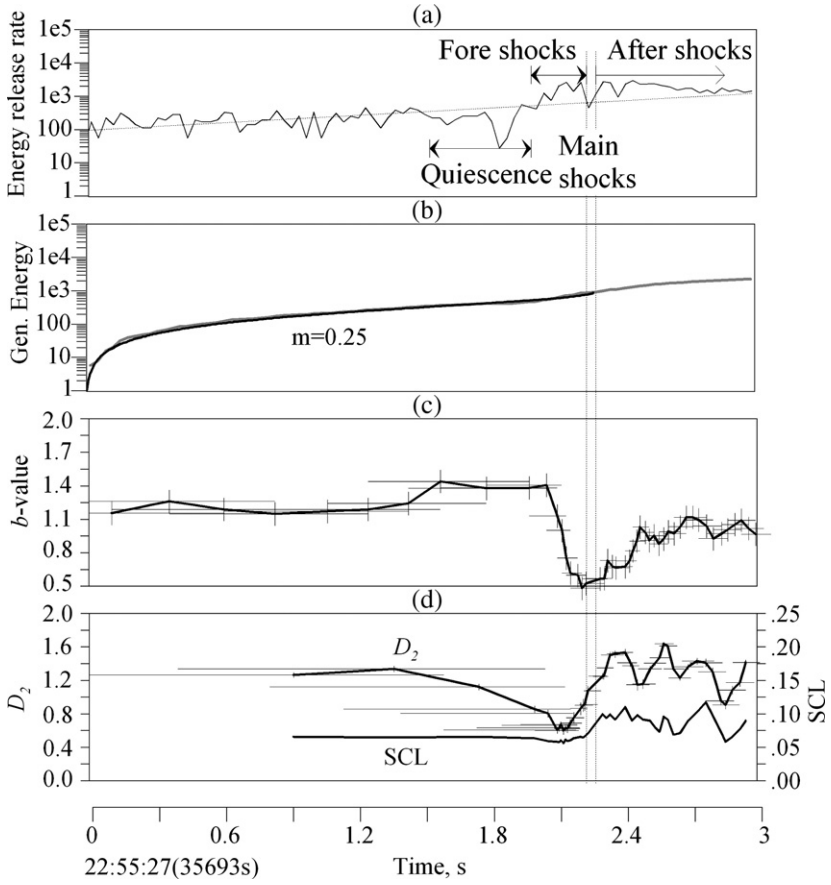

Fig. 7. Fracture of a major unbroken asperity on the through-going fault plane in a granitic porphyry sample. The AE activity reveals a typical fore-main-after shock sequence similar that observed with natural earthquakes. The *b*-values have been calculated sequentially for consecutive groups of 200 events with an increment of 50 events. The fractal dimension D_2 and SCL of the AE hypocenters have been calculated sequentially for consecutive groups of 50 hypocenters with an increment of 13 hypocenters.

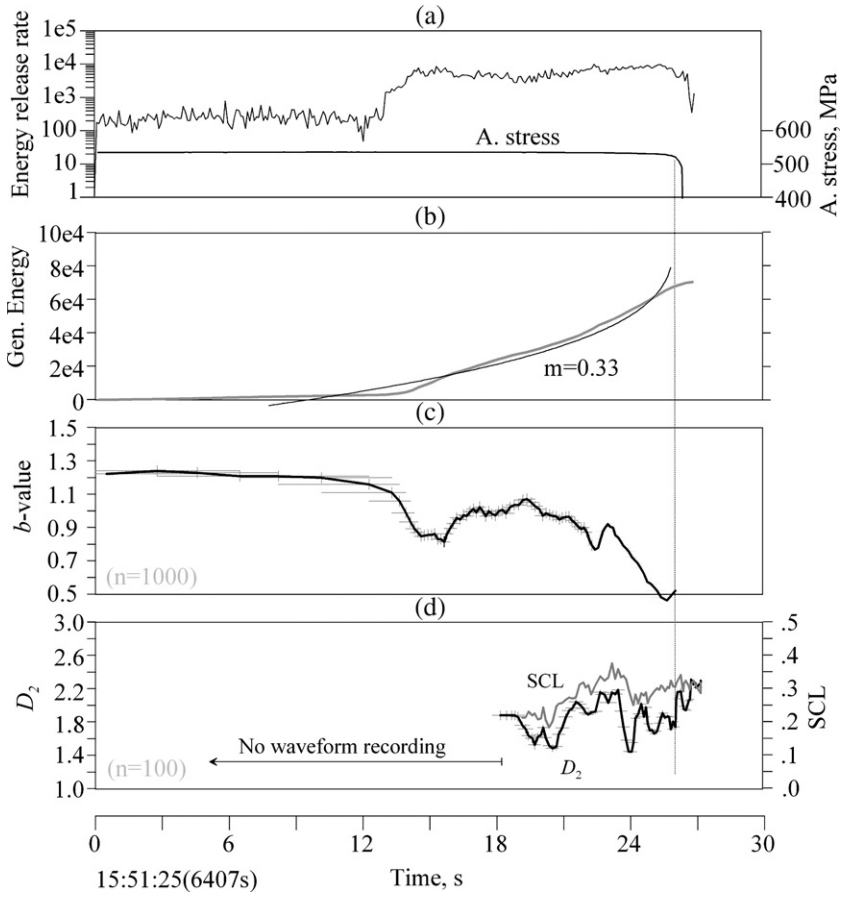

Fig. 8. Results for the coarse-grained Tsukuba granite. See text for details.

distribution of asperities in a weak fault. The mudstone samples have low strength, ~300 MPa at confining pressures of 60 MPa, and exhibit significant strain-softening features.

4. Results

As discussed previously (Lei et al., 2004; Lei, 2006), AE data obtained from rock fracture tests demonstrate that the pre-failure damage process is characterized by three typical phases of microcracking activity: the primary, secondary, and nucleation phases, respectively. The primary phase reflects the initial opening or rupture of pre-existing microcracks. The secondary phase involves the sub-critical growth of the microcrack population, manifests as increasing energy release rate and decreasing *b*-values. The nucleation phase corresponds to the initiation and accelerated growth of the ultimate fracture along either one or several incipient fracture planes. In terms of critical point concepts, the primary phase is far from the critical point. Therefore, we focus here only on the later phases, close to the critical point.

4.1. Fracture of fine-grained brittle rocks

Figs. 2 and 3 present typical results for the fine-grained hornblende schist samples. As shown in Fig. 2-b, the cumulative Benioff strain cannot be represented by a simple power-law fit. Rather, it is necessary to use either a multi-domain fit or use the log-periodic fit. Results of a multi-domain fit are illustrated here, which yield an exponent of approximately 0.27. Fig. 3 is an expanded view of the fault nucleation stage. During the final 30 or 40 s prior to global failure (critical point), the *b*-value decreases dramatically from ~1.5 to ~0.5 with several large-amplitude fluctuations. Contemporaneously, the fractal dimension and SCL show correlated temporal variations, characterized by a long-term decrease and a precursory increase prior to global failure. At the point of global failure, the axial stress dropped suddenly without any notable softening.

The decreasing fractal dimension and SCL indicate a localization of microcracks: in contrast, increasing fractal dimension and SCL reflect microcrack diffusion. Therefore, the observed temporal variations in both fractal dimension and SCL are inferred to be associated with the initiation and quasi-static growth of the ultimate fracture plane.

Figs. 4–6 represent the results for another hornblende schist sample to illustrate the generality of the observations. In addition, there is extraordinary high activity period (AE burst), marked in Fig. 5 as 'A'. Fig. 6 is a close-up view of this burst. The hypocenter distribution of the AE events during this period of time is plotted on the right side. It is observed that this dense cluster corresponds to the nuclei of the final fracture plane. From the standpoint of faulting nucleation as a homogeneous process, the evolving fracture is expected to grow progressively until failure. However, in most cases, the faulting process reveals more complicated behaviour. In the present example, a brief deceleration occurs due to fault bending (see the Discussion section for more details).

As shown in Fig. 6, the energy release, *b*-value, fractal dimension and SCL during the burst activity, demonstrate somewhat similar behaviours to a fore-main-aftershock sequence. At the point of maximum release rate, several extremely large events were observed during this

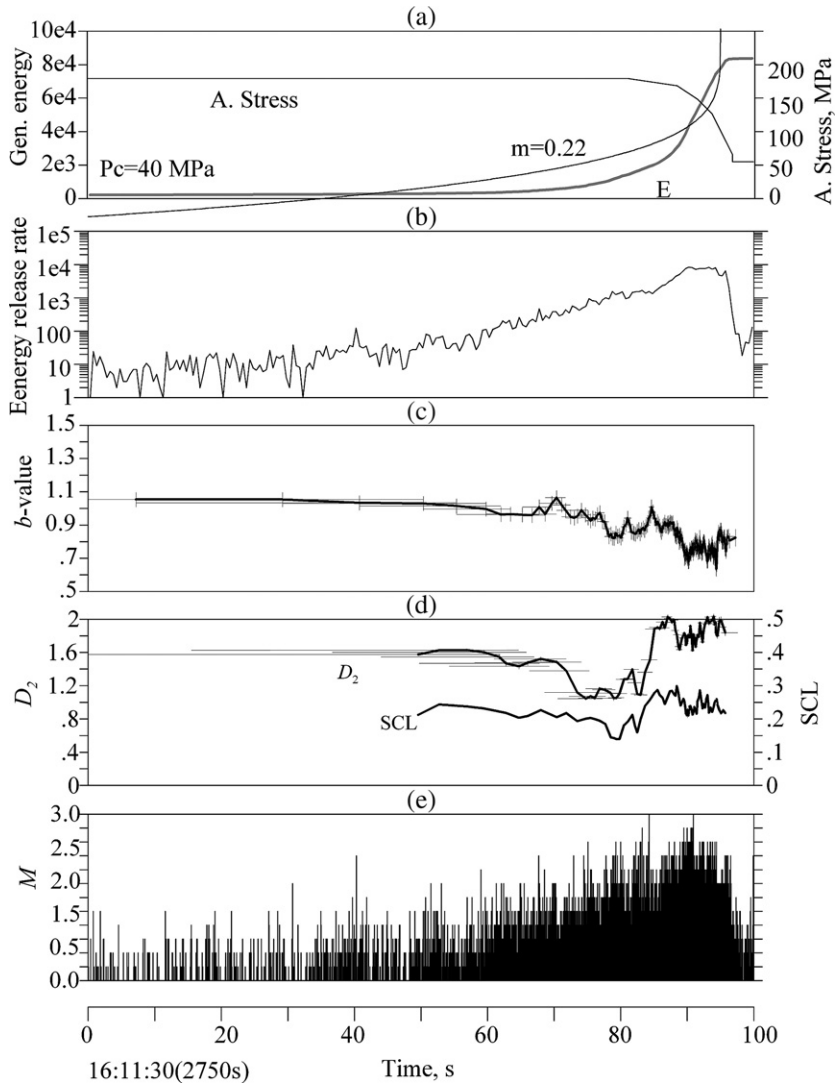

Fig. 9. Results for a typical S–C cataclasite sample. The confining pressure was kept constant at 40 MPa. a) Axial stress, cumulative energy release and power-law fit. b) Energy release rate. c) *b*-values calculated sequentially for consecutive groups of 500 events with an increment of 125 events. d) Fractal dimension D_2 and correlation length of AE hypocenters calculated sequentially for consecutive groups of 100 hypocenters with an increment of 25 hypocenters. e) Relative magnitude.

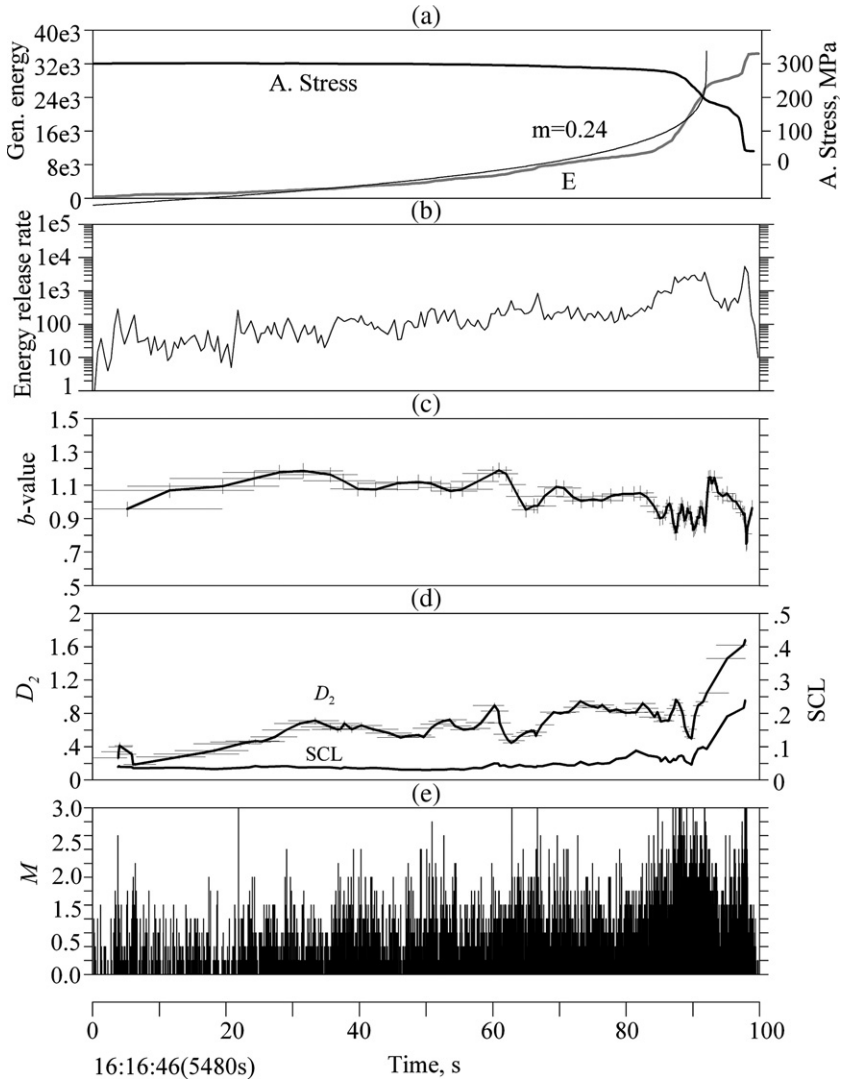

Fig. 10. Results for a ductile mudstone containing a thin, brittle quartz vein. The confining pressure was kept constant at 60 MPa. a) Differential stress, cumulative energy release and power-law fit. b) Energy release rate. c) *b*-values calculated sequentially for consecutive groups of 500 events with an increment of 125 events. d) Fractal dimension D_2 and correlation length of AE hypocenters calculated sequentially for consecutive groups of 100 hypocenters with an increment of 25 hypocenters. e) Relative magnitude.

experiment. Prior to the mainshocks, the energy release can be roughly represented by a simple power-law fit with $m=0.22$. The *b*-values, fractal dimension, and SCL show simultaneous variations: each decreases to a local minimum at the time of the main-shocks, and then gradually recovers.

Similar AE bursts were observed during the fracture of asperities on the through-going fracture plane formed in another brittle rock. Lei (2003) examined in detail the fracture of unbroken asperities in a granitic porphyry. Those AEs were caused by the fracture of individual asperities exhibiting similar characteristics to sequences of natural earthquakes, including foreshock, mainshock, and aftershock events. The increasing event rate accompanying the foreshocks and the decreasing event rate during the aftershock phase obey the modified Omori law (Lei, 2003), which is well established for earthquakes. Nucleation of the ultimate fracture corresponds to the progressive fracturing of multiple, coupled asperities on the fracture plane. Fig. 7 presents the results associated with the fracture of a single major asperity. The energy release can be represented well by a simple power-law fit with $m=0.25$. The *b*-value decreases rapidly to a local minimum at the point of the mainshocks, after which it gradually increases. The fractal dimension and SCL show local minima and precursory increases prior to the main-shocks.

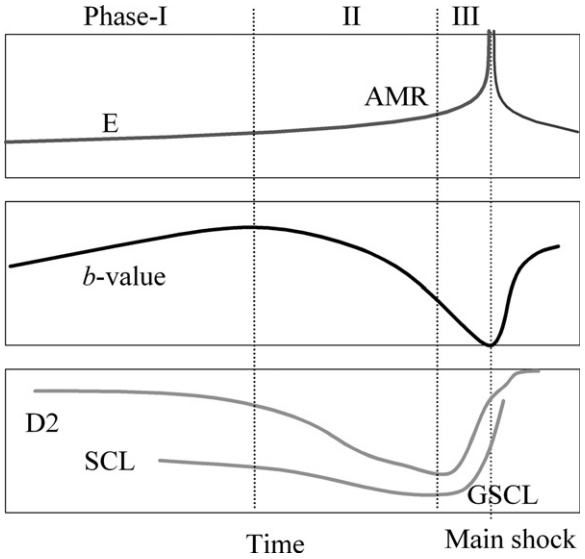

Fig. 11. Schematic diagram showing the idealized evolution of pre-failure damage as the critical point is approached.

4.2. Fracture of coarse-grained brittle rock

Fig. 8 presents the final stage of fracture in a representative coarse-grained granite, the Tsukuba granite. A small amount of strain weakening is observed prior to a sudden drop in stress. A simple power-law fit to the cumulative Benioff strain yields an exponent of 0.33. During the final ~20 s prior to global failure, the *b*-value decreases significantly from ~1.2 to ~0.5 with subsidiary fluctuations. At the same time, the fractal dimension and SCL also exhibit several fluctuations.

4.3. Fracture of S–C cataclasite

Fig. 9 presents analogous final stage results for a typical S–C cataclasite sample. The axial stress reveals significant strain weakening (Fig. 9-a). The simple power-law fit to the cumulative Benioff strain data, which results in roughly an exponent of ~0.22. During the final 40 s prior to global failure, the *b*-value decreases slightly from ~1.1 to ~0.8 with some fluctuations. Contemporaneously, the fractal dimension and SCL decrease significantly, and then increase once again. During the weakening stage, both D_2 and SCL increase significantly. The fractal dimension reaches 2.0 and maintains this level during the subsequent weakening process. The magnitudes of all events are plotted in Fig. 9-e. It is important to note that there are only a few events larger than $M=2.75$; in contrast, other lithologies produce a large number of events larger than this threshold during the final fracture stage.

4.4. Fracture of ductile mudstone containing brittle quartz veins

The general fracturing behaviors of several mudstone samples containing brittle quartz veins were presented by Lei et al. (2000c), who found that the quartz veins act as strong asperities in a weak fault. Mudstones exhibit ductile deformation under differential compression and rupture along bedding planes does not generate observable AEs. As a result, almost all the AE hypocenters are located at the intersections of the veins and the main fracture planes or sub-fracture planes (Lei et al., 2000c). Fig. 10 presents the results of a new analysis performed using data obtained from a typical experiment. The axial stress, which shows significant strain weakening, is plotted in Fig. 10-a. The cumulative Benioff strain can be partially represented using a simple power-law fit, which results in an exponent of ~0.24. During the final 40 s prior to global failure, the *b*-value decreases slightly from ~1.1 to ~0.8 with some fluctuations. At the same time, the fractal dimension and SCL undergo long-term increases. During the weakening stage, both D_2 and SCL increase significantly. Since the quartz veins occupy only a small area of the fracture plane, deformation localization is limited to the weak portions of the mudstone. Notwithstanding this, stress is nevertheless concentrated at the veins and the AEs reflect fracture of those brittle veins.

5. Discussion

5.1. Complexity in the critical point behavior prior to rock failure

It is clear that the energy release, seismic *b*-value, fractal dimension and SCL of the hypocenter distribution are all functions of the time-to-failure. Therefore, it might be expected that such parameters could be used as indicators of the critical point. However, each parameter exhibits large-amplitude fluctuations superimposed on longer-term variations. Such fluctuations are presumably governed by many factors.

First, the complexity in the characteristics of pre-failure damage stems from the non-homogeneity of the test sample. It has been proposed that the fracture of non-homogeneous rock demonstrates hierarchical properties (Lei et al., 2003). Quasi-static nucleation of faults represents dynamic fracture of asperities on the fault plane; likewise, a quasi-static nucleation process characterized by dynamic microcracking precedes the fracture of an asperity. Fracturing at a specific scale

involves fractures at all smaller scales. In the present study, the hierarchical fracturing is further confirmed. The fracture of an individual asperity shows similar damage evolution, in terms of all the measured parameters, to the global failure of the sample. In this study, the overall pre-failure damage shows AMR behaviour and the largest events in the pre-failure damage show also AMR behaviour. As a result, the hierarchical properties of the pre-failure damage lead to fluctuations in all observable parameters. The AMR model incorporating a log-periodic correction is expected to prove useful in modelling these fluctuations. Since the critical point model is based on the assumption of self-similarity, it works very well in idealized cases, where the heterogeneity at all scales is self-similar. However, even in such idealized cases, self-similarity may break down during the final stage due to the initiation and growth of the ultimate fracture plane due to following mechanisms.

Second, the micro-mechanisms of shear fracture may also lead to complexity in pre-failure damage. It has been observed in the laboratory that the evolving shear fault is guided by a process-zone at the rupture front (Cox and Scholz, 1988; Vermilye and Scholz, 1998; Zang et al., 2000; Lei et al., 2000a). The progressive activation of tensile microcracks in this process-zone leads to the growth of the shear fault overall (Lei et al., 2000a). Since tensile cracks in the process-zone have dominant orientations that differ significantly from the ultimate orientation of the macroscopic fault, the process-zone mechanism results naturally in local bends and en-echelon structures near the shear fault. Therefore, the shear fracturing process generally demonstrates complicated features even in very homogeneous rocks.

Third, it is difficult to force the rupture process into a continuous self-similar corset. For different time windows different factors may dominate the fracture process. Particularly at the final nucleation stage, fracturing associates with relative large scale, which may be out of the bound of similarity. In general, weaker areas and smaller asperities can rupture earlier than stronger areas and larger asperities, and the rupture can be obstructed at the boundary of a strong asperity. High activity of microcracking may then occur in the strong asperity after a short hiatus. A stronger asperity will therefore result in a longer hiatus and consequently higher event rate and lower *b*-value after the hiatus. As showed in Figs. 6 and 7, when an asperity is fractured, aftershocks occur in the asperity area in a relatively lower shear stress environment, resulting in a higher *b*-value. In addition, unknown microphysical source or crack interaction mechanisms may also produce the fluctuations of *b*-value and other parameters. If at one stage in the loading process of rock a new mechanism is activated one might escape from the hierarchical order of fracture which was valid until this stage was reached. This may be one reason why every parameter investigated shows very complicated temporal evolution when looked at different time resolutions.

5.2. Geophysical meaning of the study of laboratory-scale rock failure

The study of rock failure is a subject of widespread interest, with relevance to both artificial applications such as optimization of geothermal recovery, oil recovery, safe design of nuclear waste repositories, and rock bursts, and natural processes such as volcanism and seismology. In all these problems, it is important to be able to predict the time, location and intensity of potential rock fracture. Up to now, the seismic *b*-value in the magnitude-frequency distribution has been investigated by many seismologists. By comparing *b*-values for long-term seismicity and foreshocks occurring within hours and days before a mainshock, Molchan et al. (1999) found that the *b*-value drops by 0.5 during the foreshock period. This result and many other results on foreshocks represent a statistical average, and may not be characteristic of the behavior of individual foreshock sequences. However, following the development of seismic observation, there are increasing reports on premonitory decrease of *b*-value before large earthquakes in areas with dense seismic stations. For example, in the Kanto region and other areas in Japan, decreasing *b*-values prior to many earthquakes of $M \geq 5.5$ have been confirmed (Imoto, 1991; Imoto and Yamamoto, 2006). Clear premonitory anomalies in seismicity rate, *b*-value and fractal dimension with time in the 2–3 years before the 1995 Hyogo-ken Nanbu earthquake have been reported by Enescu and Ito (2001). These anomalies, characterized by increasing seismicity rate, decreasing *b*-value ($\sim$1.0 to $\sim$0.7) and fractal dimension ($\sim$1.9 to $\sim$1.3), are similar with our experimental results.

Besides the *b*-vale, *m*-value in the AMR model also shows similarity between AEs and earthquakes. In the present study, *m*-values are typically 0.2–0.3, which is consistent with that obtained from earthquakes as described in the introduction section. Therefore, statistical parameters such as *b*-value, fractal dimension, *k*-value in GSCL, and *m*-value in AMR, can be used to link experimental studies in laboratory scale and geophysical studies in large scale. Careful studies of the critical point behavior prior to rock failure in the laboratory

under controllable conditions may guide future studies on geophysical events. The critical point behavior may provide an opportunity potentially making it possible to recognize the final stage before a large event. Furthermore, experimental study is helpful for understanding the physical mechanisms behind every premonitory phenomenon thus facilitating prediction of large earthquakes, rock bursts and volcanic eruptions.

6. Conclusion

In conclusion, we have made simultaneous measurements of the energy release, seismic *b*-value, fractal dimension and SCL accompanying pre-failure damage during rock fracture tests and examined AE catalogs obtained for several common lithologies. Our results indicate that each parameter is a function of the temporal distance to the critical point and thus can potentially be used as an indicator of that critical point. As shown in Fig. 11, it is clear that the pre-failure damage evolution prior to a catastrophic failure is generally characterized by: 1) accelerated energy release, 2) a decrease of the fractal dimension and SCL with a subsequent precursory increase, and 3) a decrease in *b*-value from ~1.5 to ~0.5 for hard rocks and from ~1.1 to ~0.8 for soft rocks such S–C cataclasite. However, each parameter exhibits a complicated temporal evolution due, we suggest, either to the heterogeneity of the lithology or to the micromechanical processes of shear fracturing. Therefore, an integrated analysis of two or more parameters may lead to more effective means of predicting the time of the critical point, or in other words, the occurrence of the catastrophic event than using single parameters. The decreasing *b*-value and increasing energy release may prove meaningful for intermediate-term prediction, while the precursory increase in fractal dimension and SCL may facilitate short-term prediction.

Acknowledgments

This work was partially supported by the Joint Earthquake Science Foundation under Contract No.104146 and the National Basic Research Program of China 2004CB418405. We thank Arno Zang and the anonymous referee for their helpful comments on improving the quality of the present work.

References

Andrë, M., Lei, X.-L., Nishizawa, O., 2005. Prediction scheme for the catastrophic failure of highly loaded brittle materials or rocks. J. Mech. Phys. Solids 53, 2435–2455.

Anifrani, J.C., Le Floch, C., Sornette, D., Souillard, B., 1995. Universal log-periodic correction group scaling for rupture stress prediction from acoustic emission. J. Phys. I France 5, 631–638.

Bowman, D.D., G., King, C.P., 2001. Accelerating seismicity and stress accumulation before large earthquakes. Geophys. Res. Lett. 28, 4039–4042.

Bowman, D.D, Quillon, Sammis, G.C.G., Sornette, A., Sornette, D., 1998. An observational test of the critical earthquake concept. J. Geophys. Res. 103 (B10), 24359–24372.

Brehm, D.J., Braile, L.W., 1998. Intermediate-term earthquake prediction using the precursory events in the New Madrid seismic Zone. Bull. Seismol. Soc. Am. 88, 564–580.

Brehm, D.J., Braile, L.W., 1999. Intermediate-term earthquake prediction using the modified time-to-failure method in south California. Bull. Seismol. Soc. Am. 89, 275–293.

Bruce, A., Wallace, D., 1989. Critical point phenomena: universal physics at large length scales. In: Davis, P. (Ed.), The New Physics. Cambridge Univ. Press, New York, pp. 236–267.

Bufe, C.G., Varnes, D.G., 1993. Predictive modeling of the seismic cycle of the Greater San Francisco Bay Region. J. Geophys. Res. 98, 9871–9883.

Bufe, C.G., Nishenko, S.P., Varnes, D.J., 1994. Seismicity trends and potential for large earthquakes in the Alaska-Aleutian region. Pure Appl. Geophys. 142, 83–99.

Cox, S.J.D., Scholz, C.H., 1988. Rupture initiation in shear fracture of rocks: an experimental study. J. Geophys. Res. 93, 3307–3320.

Enescu, B., Ito, K., 2001. Some premonitory phenomena of the 1995 Hyogo-Ken Nanbu (Kobe) earthquake: seismicity, *b*-value and fractal dimension. Tectonophysics 338, 297–314.

Frohlich, C., Davis, S.D., 1990. Single-link cluster analysis as a method to evaluate spatial and temporal properties of earthquakes. Geophys. J. Int. 100, 19–32.

Gutenberg, B., Richter, C.F., 1954. Seismicity of the Earth. Princeton Univ. Press, Princeton, N.J.

Hirata, T., 1987. Omori's power law aftershock sequences of microfracturing in rock fracture experiment. J. Geophys. Res. 92, 6215–6221.

Imoto, M., 1991. Changes in the magnitude-frequency *b*-value prior to large ($M>6.0$) earthquakes in Japan. Tectonophysics 193, 311–325.

Imoto, M., Yamamoto, N., 2006. Verification test of the mean event size model for moderate earthquakes in the Kanto region, central Japan. Tectonophysics 417, 131–140.

Jaume, S.C., Sykes, L.R., 1999. Evolving towards a critical point: a review of accelerating seismic moment/energy release prior to large and great earthquakes. Pure Appl. Geophys. 155, 279–306.

Kagan, Y.Y., Jackson, D.D., 1991. Long-term earthquake clustering. Geophys. J. Int. 104, 117–133.

Lei, X.L., 2003. How do asperities fracture? An experimental study of unbroken asperities. Earth Planet. Sci. Lett. 213, 345–357.

Lei, X.L., 2006. Typical phases of pre-failure damage in granitic rocks under differential compression. In: Cello, G., Malamud, B.D. (Eds.), Fractal Analysis for Natural Hazards, Geological Society, vol. 261. Special Publication, London, pp. 11–29.

Lei, X.-L., Kusunose, K., Rao, M.V.M.S., Nishizawa, O., Satoh, T., 2000a. Quasi-static fault growth and cracking in homogeneous brittle rock under triaxial compression using acoustic emission monitoring. J. Geophys. Res. 105, 6127–6139.

Lei, X.-L., Kusunose, K., Nishizawa, O., Cho, A., Satoh, T., 2000b. On the spatio-temporal distribution of acoustic emission in two granitic rocks under triaxial compression: the role of pre-existing cracks. Geophys. Res. Lett. 27, 1997–2000.

Lei, X.-L., Nishizawa, O., Kusunose, K., Cho, A., Satoh, T., 2000c. On the compressive failure of shale samples containing quartz-healed joints using rapid AE monitoring: the role of asperities. Tectonophysics 328, 329–340.

Lei, X.-L., Kusunose, K., Satoh, T., Nishizawa, O., 2003. The hierarchical rupture process of a fault: an experimental study. Phys. Earth Planet. Inter. 137, 213–228.

Lei, X.L., Masuda, K., Nishizawa, O., Jouniaux, L., Liu, L., Ma, W., Satoh, T., Kusunose, K., 2004. Three typical stages of acoustic emission activity during the catastrophic fracture of heterogeneous faults in jointed rocks. J. Struct. Geol. 26, 247–258.

Liakopoulou-Morris, F., Main, I.G., Crawford, B.R., 1994. Microseismic properties of a homogeneous sandstone during fault nucleation and frictional sliding. Geophys. J. Int. 119, 219–230.

Main, I.G., Meredith, P.G., 1991. Stress corrosion constitute law as a possible mechanism of intermediate-term and short-term seismic quiescence. Geophys. J. Int. 107, 363–372.

Main, I.G., Meredith, P.G., Jones, C., 1989. A reinterpretation of the precursory seismic *b*-value anomaly from fracture mechanics. Geophys. J. 96, 131–138.

Main, I.G., Sammonds, P.R., Meredith, P.G., 1993. Application of a modified Griffith criterion to the evolution of fractal damage during compressional rock failure. Geophys. J. Int. 115, 367–380.

Molchan, G.M., Kronrod, T.L., Nekrasova, A.K., 1999. Immediate foreshocks: time variation of the *b*-value. Phys. Earth Planet. Inter. 111, 229–240.

Ouillon, G., Sornette, D., 2000. The concept of 'critical earthquakes' applied to main rockbursts with time-to-failure analysis. Geophys. J. Int. 143, 454–468.

Scholz, C.H., 1968. The frequency–magnitude relation of microcracking in rock and its relation to earthquakes. Bull. Seismol. Soc. Am. 58, 399–415.

Sornette, D., 1998. Discrete scale invariance and complex dimensions. Phys. Rep. 29, 239–270.

Sornette, A., Sornette, D., 1990. Earthquake rupture as a critical point, consequences for telluric precursors. Tectonophysics 179, 327–334.

Tyupkin, Yu.S., Giovambattista, R.Di, 2005. Correlation length as an indicator of critical point behavior prior to a large earthquake. Earth Planet. Sci. Lett. 230, 85–96.

Vermilye, J.M., Scholz, C.H., 1998. The process zone: a microstructural view of fault growth. J. Geophys. Res. 103 (B6), 12223–12237.

Yamashita, T., Knopoff, L., 1989. A model of foreshock occurrence. Geophys. J. 96, 389–399.

Yukalov, V.I., Moura, A., Nechad, H., 2004. Self-similar law of energy release before materials fracture. J. Mech. Phys. Solids 52, 453–465.

Zang, A., Wagner, F.C., Stanchits, S., Janssen, C., Dresen, G., 2000. The fracture process zone in granite. J. Geophys. Res. 105 (B10), 23651–23661.

Zöller, G., Hainzl, S., Kurths, J., 2001. Observation of growing correlation length as an indicator for critical point prior to large earthquakes. J. Geophys. Res. 106, 2167–2175.